PRELIMINARY EXPERIMENTS WITH A VELOCITY-SELECTED ATOMIC-BEAM APPARATUS

by Eugene J. Manista and John W. Sheldon

Lewis Research Center

Cleveland, Ohio

PRELIMINARY EXPERIMENTS WITH A VELOCITY-

SELECTED ATOMIC-BEAM APPARATUS

By Eugene J. Manista and John W. Sheldon

Lewis Research Center
Cleveland, Ohio

NATIONAL AERONAUTICS AND SPACE ADMINISTRATION

PRELIMINARY EXPERIMENTS WITH A VELOCITY-

SELECTED ATOMIC-BEAM APPARATUS

by Eugene J. Manista and John W. Sheldon

Lewis Research Center

12 442

SUMMARY

An atomic-beam apparatus has been designed and constructed for the study of velocity dependent total collision cross sections at thermal energies. The beam may be velocity selected over the range of 7×10^3 to 1×10^5 centimeters per second to provide an intense, monoenergetic (velocity spread at half-maximum calculated $\approx$ 5 percent) beam of atoms. The effect of atomic scattering by a cloud of beam atoms near the source slit is investigated.

Absolute total collision cross sections for the cesium-nitrogen $(Cs-N_2)$ and cesium-argon (Cs-Ar) interactions were measured by total beam attenuations with an angular resolution of 3.2 minutes. The cesium beam temperature was 447° K and the scattering gas temperature was 293° K. A "hard-sphere" cross section of 710×10^{-16} square centimeter was measured for the $Cs-N_2$ interaction and a cross section of 700×10^{-16} square centimeter for the Cs-Ar interaction. The absolute values of the cross sections are accurate to ± 10 percent.

INTRODUCTION

Atomic-beam techniques (refs. 1 and 2) provide a powerful tool for the investigation of many fundamental problems in modern physics. In particular, it is especially well suited for the study of the interaction of one atomic system by another. The attenuation of the beam as it passes through a region containing a scattering gas is related to the atom-scattering-gas collision cross section. The cross section so determined, however, is dependent on the efficiency of detecting small-angle collisions between the beam atoms and the scattering gas atoms.

Previous investigators (refs. 3 and 4) have shown that the velocity distribution present in an atomic beam of atoms effusing from a slit in an isothermal enclosure is Maxwellian under certain conditions of oven slit width and source pressure. Both Miller and Kusch (ref. 3) and Estermann, et al. (ref. 4) have detected appreciable deficiencies of the lower velocity groups as the source pressure is raised to increase the total beam intensity. The deficiencies in the lower velocity groups are attributed to the formation of a cloud of beam atoms near the source slit that destroys the Maxwellian distri-

bution in the beam by an effective velocity-dependent scattering. Hostettler and Bernstein (ref. 5) describing their high-transmission high-resolution slotted-disk velocity selector report a deficiency in the slower velocity groups and also in the higher velocity groups. They point out that although their source is not expected to yield a Maxwellian distribution, the deficiency in the higher velocity groups is unexplainable.

The main objective of this investigation was the determination of the effect of oven slit width and oven temperature on the deficiency of the high and low velocity groups of the beam velocity distribution. A secondary objective was the determination of the effective scattering cross sections of the cesium-nitrogen ($Cs-N_2$) and cesium-argon ($Cs-Ar$) interactions. The design of a versatile atomic-beam apparatus is presented herein. The facility can be used as a single beam with or without velocity selection. The beam may be attenuated along the beam path. This report presents the results of the initial experiments using this beam apparatus.

SYMBOLS

a	hard-sphere collision radius in Massey-Mohr formulation, cm
d	disk thickness, cm
$F(\xi)$	function that takes into account velocity distribution of beam atoms on observed probability $P(v)$
G	geometrical transmission of velocity selector
I_o	total beam intensity, atoms/(sec)(sq cm)
$I(p)$	beam intensity for pressure p of scattering gas, atoms/(sec)(sq cm)
$I(v)$	velocity-selected velocity distribution, atoms/(sec)(sq cm)
$I(v_o)$	transmitted portion of velocity distribution, atoms/(sec)(sq cm)
$I(x)$	reduced velocity-selected velocity distribution, atoms/(sec)(sq cm)
$I(0)$	beam intensity for zero pressure of scattering gas, atoms/(sec)(sq cm)
$I_i(v)$	beam velocity distribution in effusing Maxwellian gas, atoms/(sec)(sq cm)
$\bar{I}(x)$	normalized reduced velocity-selected velocity distribution
k	Boltzmann's constant, ergs/$^\circ$K
L	distance between end disks, cm
l	distance from oven slit to detector, cm

l_{cd} distance from collimating slit to detector plane, cm

l_{sc} distance from source slit to collimating slit, cm

l_1 slit width, cm

l_2 land width, cm

m atomic or molecular mass, g

n_G density of scattering atoms at temperature T_G corresponding to scattering gas pressure p, atoms/cu cm

$P(v)$ probability that beam atom of velocity v will travel distance l without scattering from beam

p pressure of scattering gas, mm Hg

p_0 reduced pressure at 1 mm Hg

$\langle p_0 \lambda_0 \rangle$ experimentally determined constant, (mm Hg)(cm)

R radial distance to slit radial midpoint, cm

$\mathcal{R}$ velocity resolution of velocity selector

r disk radius at slit half-length, cm

T absolute temperature, °K

$T(v)$ velocity dependent transmissivity, cm/sec

t transit time between end disks, sec

v velocity, cm/sec

v_m most probable velocity of velocity-selected distribution, cm/sec

v_{max} maximum transmitted velocity, cm/sec

v_{min} minimum transmitted velocity, cm/sec

v_0 peak transmitted velocity, cm/sec

x reduced velocity equal to v/v_m

α most probable velocity in beam source, cm/sec

β velocity-selector design parameter

γ velocity-selector design parameter

η	Saha-Langmuir surface ionization efficiency
Θ	collision frequency for beam atom of velocity v in hard-sphere Maxwellian scattering gas, collisions/sec
θ	minimum detectable angle of scattering out of beam angular resolution, radians
$\lambda(v)$	mean free path for velocity v at scattering gas pressure p, cm
$\lambda_0(v)$	reduced mean free path for velocity v at pressure of 1 mm Hg, cm
ξ	reduced scattering gas and beam atom parameter
$\pi \sigma_{AG}^2$	effective hard-sphere collision cross section, sq cm
σ_{AG}	effective hard-sphere collision radius, cm
Φ	surface work function in energy units, ergs
Φ_i	atom ionization potential energy, ergs
φ	slit offset angle, radians
φ_{exp}	experimentally determined slit offset angle, radians
$\psi\left[v_A\left(\dfrac{m_G}{2kT_G}\right)^{1/2}\right]$	function that takes into account motion of scattering gas on collision frequency Θ
Ω	rotational velocity of velocity-selector rotor, rotations/sec
Ω_{max}	rotational velocity of velocity selector that transmits peak velocity of distribution, rotations/sec
ω	rotational speed of velocity-selector rotor, radians/sec
ω_{sc}	width of scattering chamber entrance slit, cm
$\omega_{1/2}$	width of beam profile at half-intensity at detector plane, cm

Subscripts:

A	beam atom
G	scattering gas

4

Figure 1. - Beam apparatus, vacuum chamber, and pumping station.

C-69486

C-69487

Figure 2. - Beam apparatus on experimental mounting plate (outside of chamber) showing details of oven, velocity selector, collimating slits, atom detector, and liquid-nitrogen cold traps (aluminum baffle removed for clarity).

APPARATUS

General Characteristics of Atomic-
Beam Installation

Figure 1 shows the entire atomic-beam experimental installation. One of the unique features of this installation is the enclosure of the entire apparatus (oven, velocity selector, atom detector, etc.) in a single vacuum chamber. Extensive cold trapping is used to prevent scattered beam particles from accumulating in the chamber and thereby raising the chamber pressure.

The beam apparatus within the vacuum chamber is mounted on a 304 stainless-steel plate 1 inch thick and approximately 24 inches square. The plate can be removed from the vacuum chamber to facilitate alinement of the beam components. Figure 2 shows the beam apparatus mounted on the plate outside the vacuum chamber. Three liquid-nitrogen reservoirs with a total capacity of 13.6 liters provide a heat sink for numerous cold baffles (omitted for clarity).

The beam is formed by molecular effusion through the slit of oven O_1 and is collimated somewhat by the fore slit (fig. 3). The beam may either be velocity selected by velocity selector V_1 or transmitted past V_1 with the full distribution of velocities present in the beam. The velocity selected beam or the full beam is further collimated by the moveable collimating slit and is finally detected by atom detector D_1.
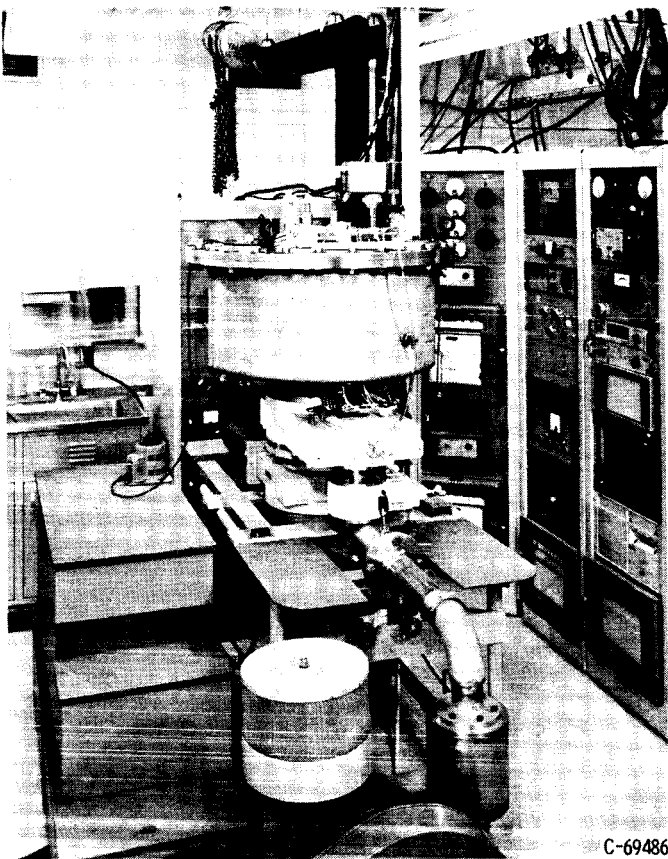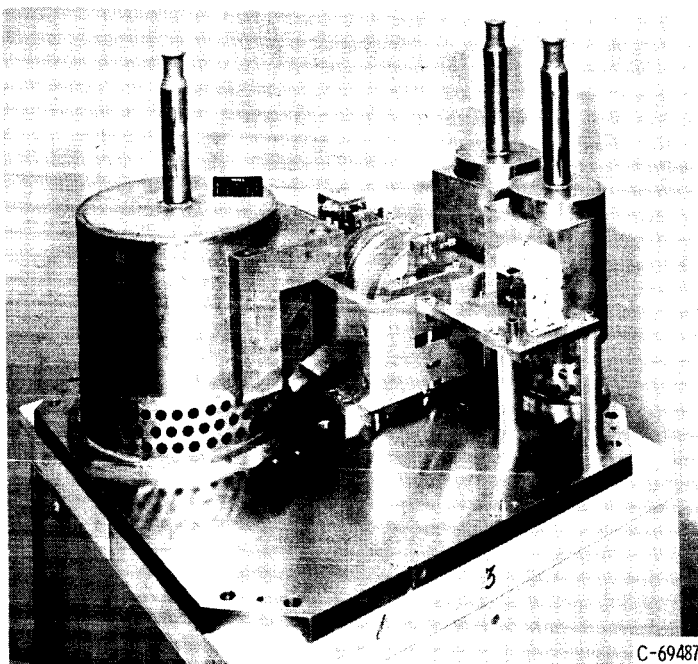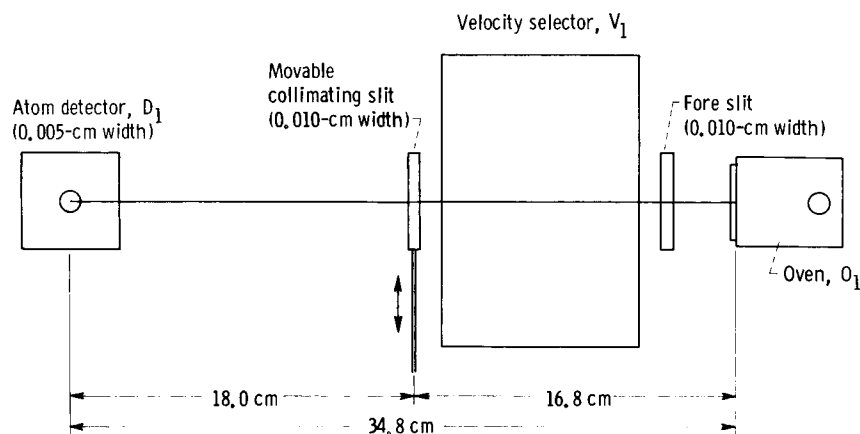
5

Figure 3. - Schematic drawing of beam apparatus.

Vacuum Chamber

The fundamental feature of an atomic beam is that, by introducing col-
limating slits at various distances from the beam source, a very narrow beam of
atoms can be formed. Since collisions with residual gas atoms effectively
destroy the directed property of the beam and also diminish the beam intensity,
it is essential that the mean free path of the beam atoms in the apparatus be
long compared with the beam length. This requires a vacuum of the order of 10^{-6}
millimeter of mercury or less. A description of the main vacuum chamber
and pumping station is given in the following paragraphs.

The beam apparatus mounting plate is bolted to four stainless-steel
blocks. The blocks are welded to the bottom plate and sides (0.0375-in.-thick
wall) of a 20-inch-deep 32-inch inside-diameter stainless-steel vacuum tank.
The lid of the chamber is a 1-inch-thick plate of stainless steel, 38 inches
in diameter, which is sealed to the chamber by a single 32-inch-diameter
O-ring. All welds, both on the inside and outside of the chamber, are of the
heliarc type.

Wilson type rotating vacuum seals, placed in the walls of the chamber, are
used to seal the shafts of the movable collimating slits and the mechanism
for raising and lowering the velocity-selector rotor. All O-ring seals
performed satisfactorily at pressures of 10^{-7} millimeter of mercury.

An 11-inch-diameter quartz viewing window, 1 inch thick, is located in
the lid and sealed to the lid by an O-ring. The window allows visual observa-
tion of the velocity selector during the experimental runs. The lid also
contains the necessary vacuum seals for auxiliary equipment, such as the filler
tubes of the cold traps, the beam shutter actuators, the atom-detector current
probes, and the oven capsule plunger mechanisms. All vacuum seals in the lid
are of either the Wilson design or the standard compression O-ring type.

The liquid-nitrogen filler tubes are of double-walled construction with the
interspace evacuated for thermal insulation. Commercially available resistance

. heating tape is used around each filler O-ring to maintain the seal at approximately room temperature.

Electrical power leads for the velocity-selector motor, the oven cartridge heaters, and for the heating current and filament bias voltage of the atom detector are brought out the bottom of the chamber through glass to metal seals. Since it is necessary to monitor and control the local temperatures at various critical areas in the beam apparatus quite closely, auxiliary glass to metal seals are located in the chamber bottom for use as thermocouple-lead feed throughs.

The vacuum station onto which the chamber is sealed consists of a 10-inch gate valve, an automatically filled liquid-nitrogen baffle, a 4100-liter-per-second diffusion pump, and a 50-cubic-foot-per-minute roughing and backing mechanical pump. Three large liquid-nitrogen cold traps are located in the main chamber and are thermally connected to an aluminum baffle plate to increase the rate of adsorption pumping of condensable vapors. Figure 1 shows the details of the vacuum chamber and the pumping station facility.

The background pressure in the vacuum chamber is monitored by a Bayard-Alpert type ion gage located in the lid. Ion currents from the gage are read by a conventional control and sensing circuit. Electron emission currents used were usually 1 milliampere. A standard ion gage sensitivity of 10 microamperes per micron of mercury per milliampere was chosen to determine the equivalent nitrogen pressure. Pressures of the order of 1×10^{-6} millimeter of mercury can be obtained without cooling the internal liquid-nitrogen traps and aluminum baffle. After baking out all ovens at 250° C for a few hours, the pressure under actual experimental conditions is typically 3×10^{-7} millimeter of mercury with liquid nitrogen in the cold-trap reservoirs.

Velocity Selector

Theory. - A drawing of a simple rotating-disk velocity selector is shown in figure 4. Consider, for the purpose of illustration, the beam and selector disks to be of infinitesimal width. The particles in the beam that traverse the space between the disks L in a time t will get through the slit in the second disk if

$$t = \frac{\varphi}{\omega} \qquad (1)$$

where ω is the disk rotational speed and φ is the slit offset angle. Thus, this idealized selector passes particles with velocity

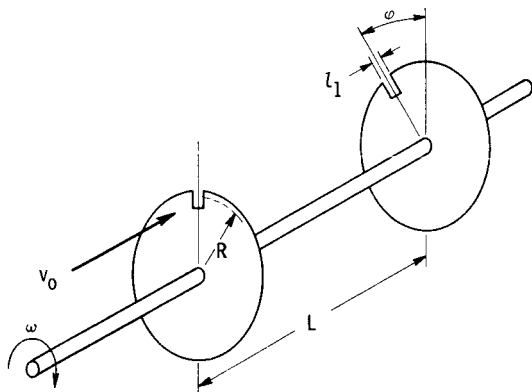$$v_o = \frac{L}{t} = \frac{L\omega}{\varphi} \qquad (2)$$

Figure 4. - Diagram of simple rotating-disk velocity selector.

Note that such a velocity selector will only pass a small fraction of the

beam particles that have velocity v_o. This fraction called the transmissivity T is given by

$$T = \frac{l_1}{2\pi R} \tag{3}$$

where R is the disk radius at the slit radial midpoint and l_1 is the slit width.

Note that this velocity selector would also pass particles with velocities v_1, v_2, etc., where

$$v_1 = \frac{L\omega}{2\pi + \varphi}, \quad v_2 = \frac{L\omega}{4\pi + \varphi}, \quad \cdots \quad v_n = \frac{L\omega}{2n\pi + \varphi} \tag{4}$$

These are called selector overtones or sidebands.

An attempt to increase T by adding more slits in this selector would increase the number of sidebands and bring them closer to the desired pass velocity. High transmissivity combined with elimination of sidebands is the challenge of velocity-selector design.

The velocity-selector design chosen for this investigation was originally presented by Hostettler and Bernstein (ref. 5). The principle is the same as for the selector illustrated in figure 4. Hostettler and Bernstein increased the transmissivity by using 278 slits per disk. Elimination of the previously
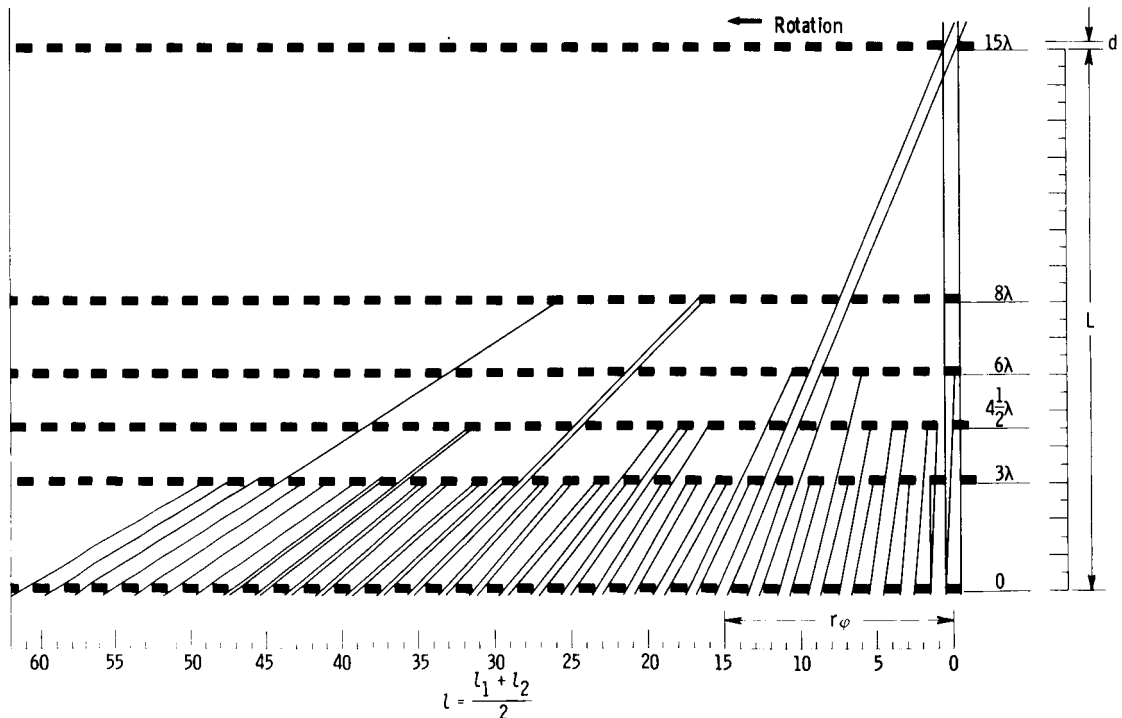

Figure 5. - "Unrolled" velocity-selector rotor (taken from ref. 5). Beam particle motion upward.

discussed sidebands was accomplished by the judicious placement of four inter-mediate disks between the two end disks.

The "channel" through which particles are permitted to pass in the slotted-disk velocity selector is shown in figure 5. This figure is a graphic representation of an "unrolled" rotor; straight lines represent particle paths in the selector with the line slope being proportional to particle velocity. Due to the finite width of this channel the particles that can get through it may have velocities in the narrow range between v_{min} and v_{max}.

Transit time considerations for an infinitely narrow beam yield

$$v_{max} = \left(\frac{L - d}{\varphi - \frac{l_1}{r}} \right) \omega \qquad (5)$$

and

$$v_{min} = \left(\frac{L + d}{\varphi + \frac{l_1}{r}} \right) \omega \qquad (6)$$

where d is the disk thickness, l_1 is the slit width, and r is the disk radius at the slit radial midpoint.

The resolution $\mathcal{R}$ of the velocity selector is defined by

$$\mathcal{R} \equiv \frac{v_{max} - v_{min}}{2 v_o} \simeq \gamma - \beta \qquad (7)$$

The geometric parameters (including γ and β) are presented in table I.

The velocity dependent transmissivity $T(v)$ is defined as the number of particles with speed v that pass through the velocity selector per incident particles with speed v. The velocity dependent transmissivity peaks at v_o and drops to zero at v_{max} and v_{min}. The transmitted velocity distribution $I(v_o)$ is given by

$$I(v_o) = \int_{v_{min}}^{v_{max}} T(v) I_i(v) dv \qquad (8)$$

where $I_i(v)$ is the distribution of particle speeds in the beam as it arrives at the velocity selector. If the atom oven contains particles with a Maxwellian speed distribution, then (ref. 6)

$$I_i(v) dv = 2 I_o \frac{v^3}{\alpha^4} e^{-(v/\alpha)^2} dv \qquad (9)$$

where I_o is the total beam intensity and $\alpha^2 = 2kT/m$, where k is Boltzmann's constant, T is the beam source oven temperature, and m is the beam particle

mass. Using this expression for $I_i(v)dv$ Hostettler and Bernstein (ref. 5) report

$$I(v_o) \simeq Gv_oI_i(v_o) \qquad (10)$$

where the geometric transmissivity factor G is defined as

$$G \equiv \left(\frac{l_1}{l_1 + l_2}\right)\gamma\left(\frac{\gamma - \beta}{\gamma}\right)^2 \qquad (11)$$

TABLE I. - VELOCITY-SELECTOR GEOMETRIC PARAMETERS

Number of disks	6
Diameter of disks	16.0 cm
Number of slits per disk	278
Radial length of slits	0.8 cm
Slit width, l_1	0.081 cm
Angle subtended by slit	0.0101 radian
Land width, l_2 (average value)	0.0905 cm
Angle subtended by land	0.0124 radian
Disk radius (O.D.)	8.0 cm
Disk radius r at slit half length	7.6 cm
Disk thickness, d	0.16 cm
Overall length of rotor, L + d	10.16 cm
Distance between end disks, L	9.997 cm
$\varphi = \frac{15}{r}\left(\frac{l_1 + l_2}{2}\right)$ (based on center of slit)	0.1695 radian
$\gamma = \frac{l_1}{r\varphi}$	0.0631
$\beta = \frac{d}{L}$	0.0163
$G = \frac{l_1}{l_1 + l_2}\gamma\left(1 - \frac{\beta}{\gamma}\right)^2$	0.0164
$R = \gamma - \beta$	0.0468

Construction. - The velocity selector is shown in figure 2. The frame was machined from aluminum. The rotor assembly is mounted in stainless-steel blocks that move vertically in the frame to allow removal of the selector rotor from the beam path. The movement of the blocks is synchronized by gears beneath the frame. The motion is transferred to the gears by a 1/4-inch-diameter stainless-steel shaft extending through a Wilson seal in the side of the vacuum chamber.

Figure 6 is a schematic drawing of the rotor assembly. All the disks are identical and are made of 2024-T3 aluminum alloy. Fourteen disk blanks were clamped together between two heavy end disks. The slits were milled on a horizontal mill by using a 0.032-inch-thick circular carbide saw. After the

10
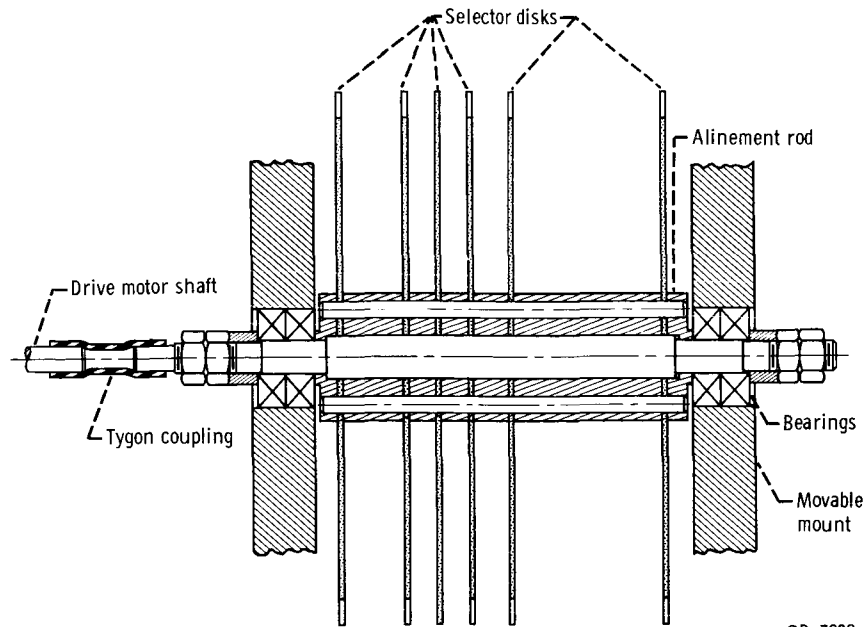
Figure 6. - Velocity-selector rotor assembly.

slits were machined, the holes for the alinement shafts were bored. The relative angular positions of these holes on the various disks were determined in accordance with the "unrolled" rotor sketch of figure 5. The holes were located by placing each disk on a jigboard with a rotary table having angular graduations down to 2 seconds of arc (0.1 percent of a slit width).

The disk spacer at the downstream end of the rotor had one-half its perimeter vapor blasted and one-half polished. This was done to facilitate signal pickup by an optical tachometer.

The bearings outer housings were press-fitted into the rotor mounting blocks. The degree of tightness on the shaft nuts determined the bearing preload.

The bearings themselves were furnished by the New Departure Company on an experimental basis. They were lubricated by impregnating the balls with molybdenum disulfide.

The rotor shaft is connected to the drive motor by a flexible coupling made of heavy-walled tubing. The drive motor, a two-phase synchronous motor, was designed to operate at speeds between 1800 and 18,000 rpm in a vacuum of 10^{-7} millimeter of mercury. The motor housing is sealed and pumped separately to prevent internal outgassing products from being released into the vacuum chamber.

Oven

The oven used is similar in design to that of the "ideal oven and slit" of Miller and Kusch (ref. 3) and is shown schematically in figure 7. The oven body is made from a solid block of oxygen-free high-conductivity copper to
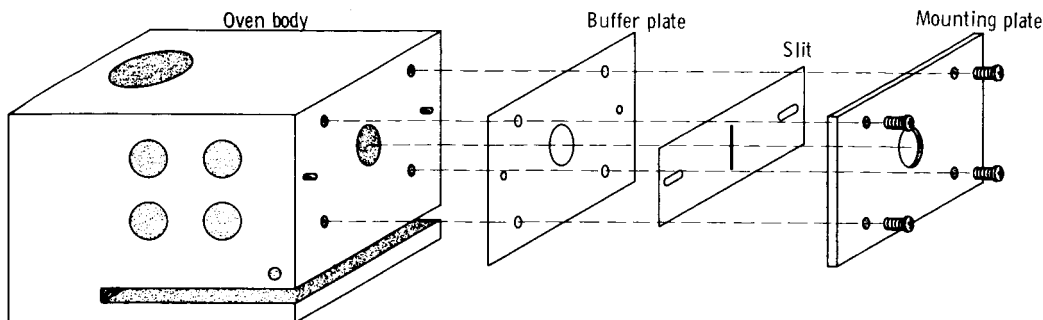
11

Figure 7. - Ideal oven and slit. Oven body is made from oxygen-free-high-conductivity copper. Remaining parts are made of 304 stainless steel.

ensure a uniform temperature throughout. The oven slit is formed from 0.0051-centimeter-thick stainless-steel shim stock in which a 0.508±0.002-centimeter-high slit of various widths has been cut by electron-beam techniques. The slit is held in alinement by accurately located dowel pins in the oven face.

During a previous test, the stainless-steel oven slit and mounting face plate became bonded to the face of the copper block after oven operation in vacuum, thus making removal of the slit assembly for oven cleaning between runs difficult. To reduce the tendency for the oven slit and mounting plate to bond to the oven face, a 0.0051-centimeter-thick stainless-steel buffer plate was introduced between the oven face and the slit assembly. No further difficulty was experienced in subsequent runs using this construction. The oven is held in alinement to the desired beam path by accurately located 0.1875-inch-diameter stainless-steel dowels in the base.

Oven cartridge heaters are made by wrapping 18 turns of 20-mil tungsten wire around a 0.125-inch-diameter ceramic core (fig. 8). Boron-nitride inserts are used to insulate elec-
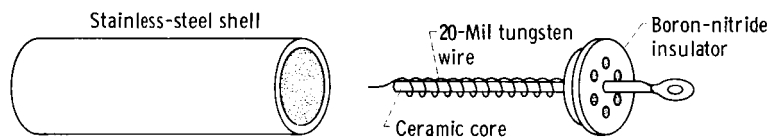

Figure 8. - Exploded schematic drawing of oven heater assembly.

trically the front and rear of the heater assembly. The heater assembly is then inserted into a 0.380-inch-diameter thin-walled stainless-steel tube 1.75 inches long. The back end of the heater coil is pulled taut to fix the front boron-nitride insulator and is silver soldered to the end of the stainless-steel tube to complete the construction. Holes are drilled through the front section of the boron-nitride insulation to allow outgassing of the heaters.

Beam material is introduced into the oven in the form of preloaded vacuum capsules. The capsules are placed in a tilted position in the oven-well reservoir before closing the chamber for pumpdown. The plunger mechanism that has proved successful consists of a stainless-steel plug that is tapered to fit tightly into the top of the oven-well reservoir opening. A 0.250-inch-diameter stainless-steel rod passes snugly through the plug into the oven well and into contact with the capsule. The upper end of the plunger rod is brought out

12

through an O-ring seal in the lid of the chamber. After baking out the oven at 250° C for several hours, the temperature of the oven is brought to the desired operating level and allowed to reach thermal equilibrium. The upper end of the plunger rod is gently tapped with a hammer until the capsule breaks. The foregoing technique has been used with complete success and minimizes the introduction of impurities into the oven material. Moreover, the seal between the copper oven and the stainless-steel plug has proved very reliable in that the loss rate of oven material seems to be entirely accountable by the efflux rate through the oven slit and is little influenced by parallel "leaks."

Atom Detector

The neutral-atom detector is a surface ionization detector that has been used extensively in atomic beam work with alkali metals (ref. 2). It consists of a hot tungsten filament across which the neutral beam passes. Alkali atoms striking the filament are ionized on the surface and the resulting ions are accelerated to a cylindrical collector surrounding the filament. The collected ion current is measured by an electrometer.

Theory. - The surface ionization process requires that the ionization potential of the incident atom be lower than the filament work function; hence, the application of the surface ionization detector is restricted to beams with low ionization potentials. This restriction is, however, one of the greatest assets of the detector; it is relatively insensitive to the background gas in the vacuum chamber.

The tungsten filament ionization efficiency η (emitted ion current divided by incident atom flux) is given as a function of temperature by the following version of the Saha-Langmuir equation (ref. 7)

$$\eta = \left\{ 1 + 2e^{-[(\Phi - \Phi_i)/kT]} \right\}^{-1} \tag{12}$$
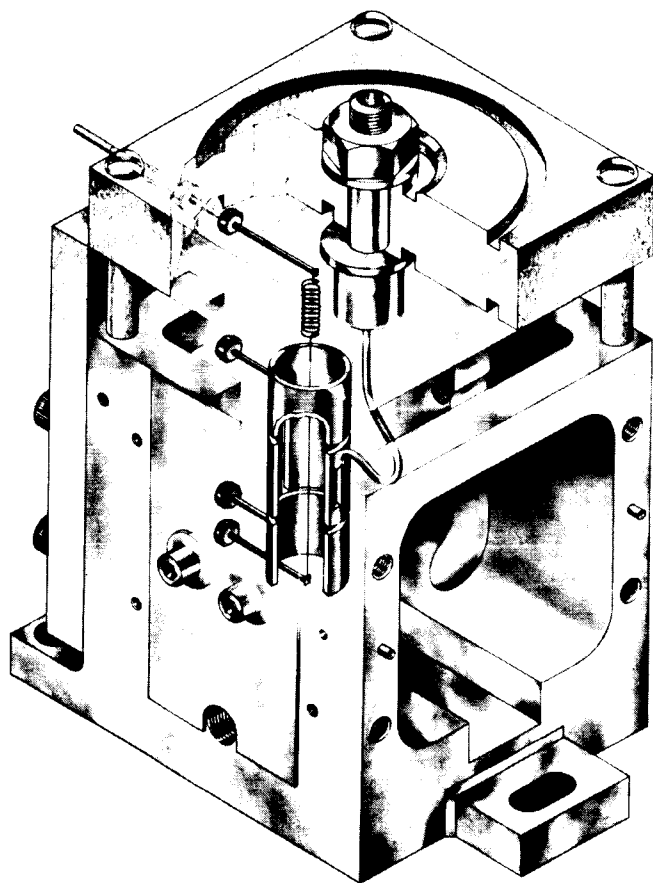
where Φ is the surface work function expressed in energy units and Φ_i is the ionization potential energy of the detected atom. This equation predicts $\eta = 1$ at $T = 0$ and decreasing η with increasing T. This functional dependence is found above a minimum temperature (1200° K for cesium on tungsten). Below this minimum temperature, the ionization efficiency for cesium on tungsten drops rapidly to zero. This is attributed to a stable adsorbed layer of cesium on the filament surface that lowers the surface work function. A high surface work function is desirable from the standpoint of obtaining η very close to 1.0. An increase in work function over the value for pure tungsten can be realized by adsorbing a layer of oxygen on the filament surface (for tungsten oxide, $\Phi = 6.24$ ev, ref. 7).

If, however, low beam intensities are to be measured with a surface ionization detector, another consideration, background ion emission, discourages the use of oxygenated tungsten filaments. The thermal emission of background alkali ion pulses from tungsten has been investigated by Minturn, Datz, and Taylor (ref. 8). They observed that a well-aged "high purity" tungsten filament emitted an ion background of approximately 10^{-10} ampere per square centi-

13

meter at a temperature of 1640° K. The emission consisted of several pulses per second; each pulse containing of the order of 10^6 ions. Mass-spectrographic analysis revealed this ion background to be composed mainly of potassium. It persisted throughout the life of the filament. The rate of emission of these background pulses increased approximately linearly with increasing oxygen pressure in the range 10^{-7} to 10^{-5} millimeter of mercury.

While the mechanism of background ion pulse emission is not well understood, it is certainly dependent on oxygen and alkali metal contamination (ref. 8).

Construction. - The detector is presented schematically in figure 9. It consists of a stainless-steel frame, a Supramica 500 insulator for mounting the ion collector, and a boron-nitride insulator for mounting the filament assembly and guard rings. The filament wire (0.0024 in. diam.) is an ultrahigh-purity tungsten reported by Roberts (ref. 9) to have a lower ion background than other commercially available products. The filament is held taut by a spring consisting of eight turns of 0.008-inch-diameter tungsten wire. The spring design is in accordance with the specifications suggested by Blodgett and Langmuir (ref. 10).

The guard rings and collector were fabricated from 0.50-inch outside-diameter 0.032-thick-wall stainless-steel tubing. The surfaces of the guard rings and the collector were highly polished. The collector has a 0.060- by 0.25-inch beam entrance hole in the side facing the beam and a 0.060-inch slit extending the length of the collector in the opposite side. This slit facilitates assembly of the detector.

The collector is supported by a stainless-steel rod mounted in a Supramica 500 insulator on top of the detector frame. The Supramica has a volume resistivity of 10^{17} ohm-centimeters. A banana jack connector is machined into the top of the support rod, which extends through the insulator.

An electrometer rigid cable mates with the banana jack connector. The cable, which is approximately 6 inches long

CD-7899

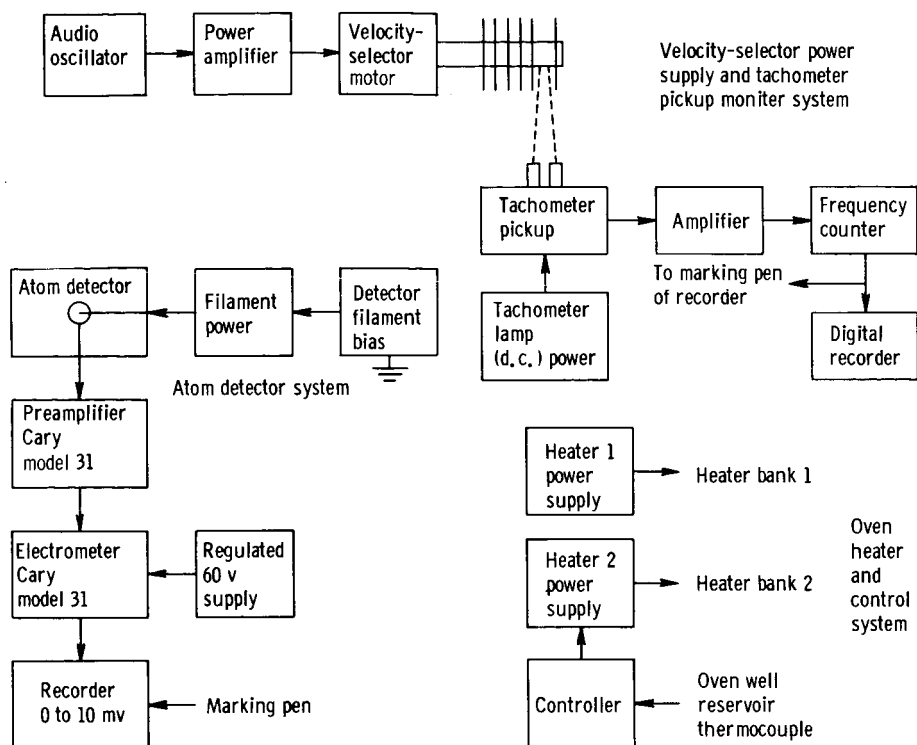Figure 9. - Cutaway view of surface ionization atom detector.

14

Figure 10. - Block diagram of instrumentation in beam apparatus.

(7/16 in. O.D.) passes through an O-ring compression seal in the vacuum chamber lid and feeds directly into the electrometer preamplifier head, which is mounted in an inverted position.

Instrumentation

General features of the instrumentation required in the beam apparatus are shown in block form in figure 10.

The variable-frequency power to operate the velocity selector is obtained from an audio-oscillator-driven power amplifier. The velocity-selector drive motor is **reactance-corrected** at various speeds by a bank of capacitors. A light-beam tachometer system is employed to determine the rotational speed of the velocity selector. A steady light beam falls on the half-dull half-polished surface of the rotor shaft and the reflected light beam is sensed by a phototube. The series of pulses from the phototube are amplified and counted for 1 second by a frequency counter. The displayed count is recorded by a digital printout system.

Two iron-constantan thermocouples are used to monitor and control the temperature of the atom oven. One thermocouple is located near the oven face slit assembly, and the other is placed near the oven-well reservoir. Two banks of heaters are used in the oven. One bank is continually on; the other is supplied on impulse heating current pulse whenever the control temperature is

15

not maintained at the preset level. The controller is capable of maintaining the oven temperature constant to within $\pm 0.25^{\circ}$ C once thermal equilibrium has been established. The oven temperature near the front slit assembly is recorded by a strip-chart recorder that has been calibrated to read from 0° to 600° C. The oven well reservoir temperature is read periodically by a room temperature compensated potentiometer, calibrated to the thermocouple system used.

An extensive iron-constantan thermocouple system monitors the temperatures at various points in the beam apparatus. The reference junction for the thermocouple system is held at 150° F by a multi-input thermocouple reference junction oven. A 10-point 0- to -10-millivolt recorder samples the temperatures periodically.

Positive or negative currents to the atom-detector collector are detected and measured by an electrometer (Applied Physics Corp. Model 31) of sensitivity $\approx 1 \times 10^{-15}$ ampere. The output of the electrometer drives a 0- to 10-millivolt strip-chart recorder. The printout signal command pulse from the frequency counter is also used to drive a marking pen on the recorder to correlate the electrometer signal with that of the frequency counter when velocity distributions are scanned.

The atom-detector filament current is obtained from a highly regulated direct-current supply. Filament voltage bias is established by batteries.

Angular Resolution

The quantum theory of atomic collisions (Massey and Mohr, ref. 11 and Massey and Burhop, ref. 12) predicts a total "hard-sphere" scattering cross section of $4\pi a^2$ when the DeBroglie wavelength associated with the colliding particles is large compared with a and where a is one-half the sum of the effective diameters of the interacting particles. The value of $4\pi a^2$ is four times that required by a classical treatment, πa^2. Furthermore, as the energy of the interacting particles increases and the DeBroglie wavelength becomes smaller, quantum theory gives a value of $2\pi a^2$, or twice the classical hard-sphere cross section of πa^2. The reason for this doubling and quadrupling of the classical cross section is due to a large forward scattering peak in the differential cross sections. Accordingly, the angular resolution of the apparatus used to determine a total collision cross section experimentally is an important parameter to be considered when comparing the results with those of a theoretical nature or another experimental value.

The angular resolution θ is a geometric property of the beam apparatus and is shown in figure 11. The calculation is presented for a scattering gas contained in a well-defined region (a scattering chamber) over a limited length of the total beam path. The results, however, can be extended to the case where the scattering gas occurs over the total length of the beam. The angle θ is defined to be that angle of scattering of the incident beam particles into the detector determined by those beam particles that would normally, in the absence of a scattering gas and with the scattering chamber slit width ω_{sc} treated as a collimating slit at the midpoint of the scattering chamber, contribute to the half-width of the beam at the detector plane. The preceding definition
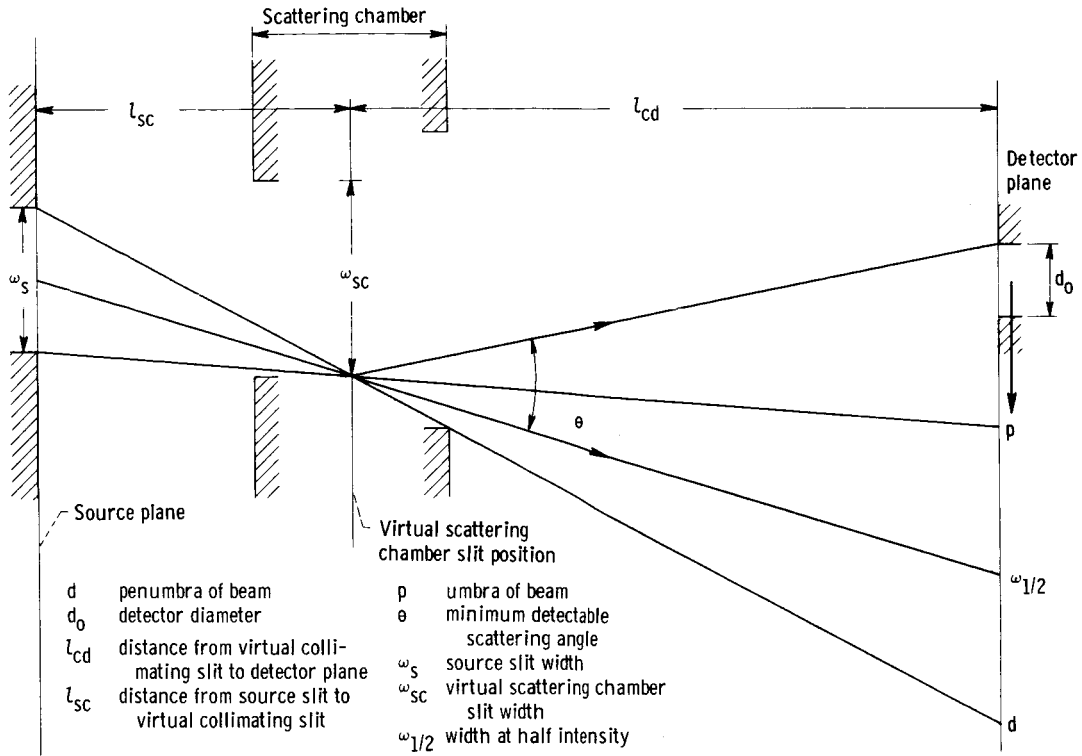
16

Figure 11. - Minimum angular resolution of beam-scattering apparatus. Scattering gas is contained in scattering chamber.

The glossary labels in the figure:

d   penumbra of beam
d_o detector diameter
l_{cd} distance from virtual colli-
         mating slit to detector plane
l_{sc} distance from source slit to
         virtual collimating slit

p   umbra of beam
θ   minimum detectable
         scattering angle
ω_s source slit width
ω_{sc} virtual scattering chamber
         slit width
$\omega_{1/2}$ width at half intensity

gives θ in radians as

$$\theta = \frac{d_o + \omega_{1/2}}{2 l_{cd}} \qquad \theta \ll 1 \qquad (13)$$

where l_{cd} is the distance from the detector plane to the midpoint of the scattering region in centimeters, d_o is the diameter of the detector in centimeters, and $\omega_{1/2}$ is the width of the beam at half-intensity at the detector plane in centimeters. Algebraic manipulation of the standard beam profile equation (ref. 1) gives the following relation for $\omega_{1/2}$

$$\omega_{1/2} = \omega_{sc}\left(1 + \frac{l_{cd}}{l_{sc}}\right) \qquad (14)$$

where l_{sc} is the distance in centimeters from the source to the midpoint of the scattering region.

In the attenuation experiments, scattering occurs over the entire beam path. The first 4 centimeters that the beam travels through the scattering gas is only about 10 percent of the total path and its effect on the angular resolution is neglected. The effective scattering chamber path length is made up of two distinct regions. Region one is that contained by the fore slit and the movable collimating slit, a distance of 12.8 centimeters, while region two is bounded by the movable slit and the detector plane, a distance of

17

18 centimeters. The results of the previous discussion are used to calculate the angular resolution associated with the two regions: $\theta_I \cong 0.80 \times 10^{-3}$ radian, and $\theta_{II} \cong 1.03 \times 10^{-3}$ radian. The two scattering regions are weighted in terms of their contribution over the entire path length, so that the nominal angular resolution becomes 3.2 minutes.

EXPERIMENTAL PROCEDURE

A cesium atomic beam was employed to evaluate the velocity selector and the oven slit design. Total beam scattering experiments were also performed with nitrogen, argon, and helium as the scattering gas. Oven slit widths of 0.010 and 0.020 centimeter were used in the velocity-selector investigations. Evacuated capsules holding about 0.27 gram of 99.95 percent pure cesium metal were used in the experimental runs.

The preliminary preparation, prior to the breaking of the capsule to produce a cesium beam, consisted of a 2-day pumpdown of the vacuum chamber to a nitrogen pressure of 1×10^{-6} millimeter of mercury. During the pumpdown, oven O_1 was baked out at 250° C for at least 24 hours. The filament of D_1 was also continually baked at a temperature of about 2000° K. The initial noise level was of the order of 10^{-10} ampere. After the 2-day pumpdown and bakeout, the oven temperature was brought to the desired level and allowed to stabilize. The D_1 filament noise was now down to about 1×10^{-13} ampere with peak to peak swings of 5×10^{-14} ampere. Liquid nitrogen was introduced into the cold-trap reservoirs, and the entire apparatus was allowed to stabilize thermally overnight.

The cesium capsules were broken at background pressures of 3×10^{-7} millimeter of mercury. No observable pressure rises ($\Delta p < 10^{-7}$ mm Hg) were noted during or after the capsules were broken. The beam intensity stabilized after 30 to 45 minutes. Velocity distributions were then taken at various oven reservoir temperatures in the range of 140° to 200° C. The data recorded were the total beam current, before and after velocity distribution scanning, the background ion detector noise, and the actual velocity distribution. The velocity distribution was scanned over a period of about 5 minutes by accelerating the velocity selector up to a rotational speed of 220 rotations per second (rps) and then by cutting off the power to the motor. The frequency counter was set to count and record the rotational speed of the velocity selector every 5 to 6 seconds. As the velocity selector slowed down due to friction (an average decrease of less than 1 rps per second was noted) the beam current measured by D_1 was recorded by the electrometer. The response time of the input circuit of the electrometer was 0.1 second. An experimental check of the method used to scan the velocity distributions in this manner was made by slowly scanning the distribution manually over a period of 30 minutes. Both methods yielded identical results.

Total beam attenuation experiments were performed with an oven slit width of 0.010 centimeter and at an oven temperature of 447° K. The scattering gases (purity $\simeq 99$ percent) were introduced into the entire chamber through a variable leak located in the chamber lid. The pressure of the scattering gas was determined by a calibrated Bayard-Alpert ion gage. The calibration of the ion

gage was performed against a McLeod gage of accuracy ±10 percent in the range of the calibration. Because of the long path length, 34.8 centimeters, 0 to 90 percent attenuation of the total beam could be achieved over the pressure range of 1×10^{-6} to 10×10^{-6} millimeter of mercury. Velocity distributions were taken at scattering gas pressures corresponding to 0 and 50 percent attenuations in the Cs-N_2 and Cs-Ar experiments, and over a range of 0 to 80 percent in the cesium-helium (Cs-He) experiments.

VELOCITY-SELECTOR PERFORMANCE

The theoretical velocity distribution for a Maxwellian source of effusing atoms, after velocity selection, is given by $I(v)$:

$$I(v) = 2I_oG \frac{v^4}{\alpha^4} e^{-(v/\alpha)^2} \tag{15}$$

The peak of the distribution given in equation (15) occurs at a value of $v = v_m = \sqrt{2}\,\alpha$. For a reduced velocity $x = v/v_m$, equation (15) may be written as the following generalized distribution:

$$I(x) = 8I_oGx^4e^{-2x^2} \tag{16}$$

Normalizing equation (16) to its value at the peak $x = 1$ yields a universal reduced velocity function $\overline{I}(x)$:

$$\overline{I}(x) = \frac{8I_oGx^4e^{-2x^2}}{I(1)} \tag{17}$$

The normalized theoretical $\overline{I}(x)$, as defined in equation (17), is taken for comparison with the experimental distributions.

A total of 12 velocity distributions taken during two different runs was analyzed for comparison with the theoretical Maxwellian distribution. In order to compare the data for different oven temperatures, and also to eliminate the possible systematic errors due to a slight misalinement of the velocity-selector disks, the observed peak of the experimental distribution was chosen as the normalizing point in all cases. The velocity at the peak could be experimentally determined to within 1.4 percent. Figure 12 presents the observed distributions for various oven temperatures and the two oven slit widths used. The ordinates in figures 12(a) to (f) are $I(v/v_m)/I(v_m/v_m) = I(x)/I(1)$, where $x = v/v_m$ and v_m is the observed velocity at the peak of the distribution and where $\overline{I}(1)$ is the observed intensity at the peak. The abscissas in figures 12(a) to (f) are the corresponding values of x. The vertical bars represent the experimental errors assigned to the data, while the solid curve is the theoretical normalized Maxwellian distribution $\overline{I}(x)$.

It was observed that the absolute velocity at the peaks of the distributions was systematically occurring at higher values of Ω_{max} (higher rotational speeds of the velocity-selector rotor) than values that would be expected from the design constants of the selector. This velocity shift of the entire distribution has been traced to a misalinement of the third disk. The velocity at

the peak of the transmitted distribution, given by equation (15), is related to the oven temperature by

$$T = \frac{m}{4k} v_m^2 \qquad (18)$$

while the velocity selector transmits the peak velocity at a rotational speed of Ω_{max} given by

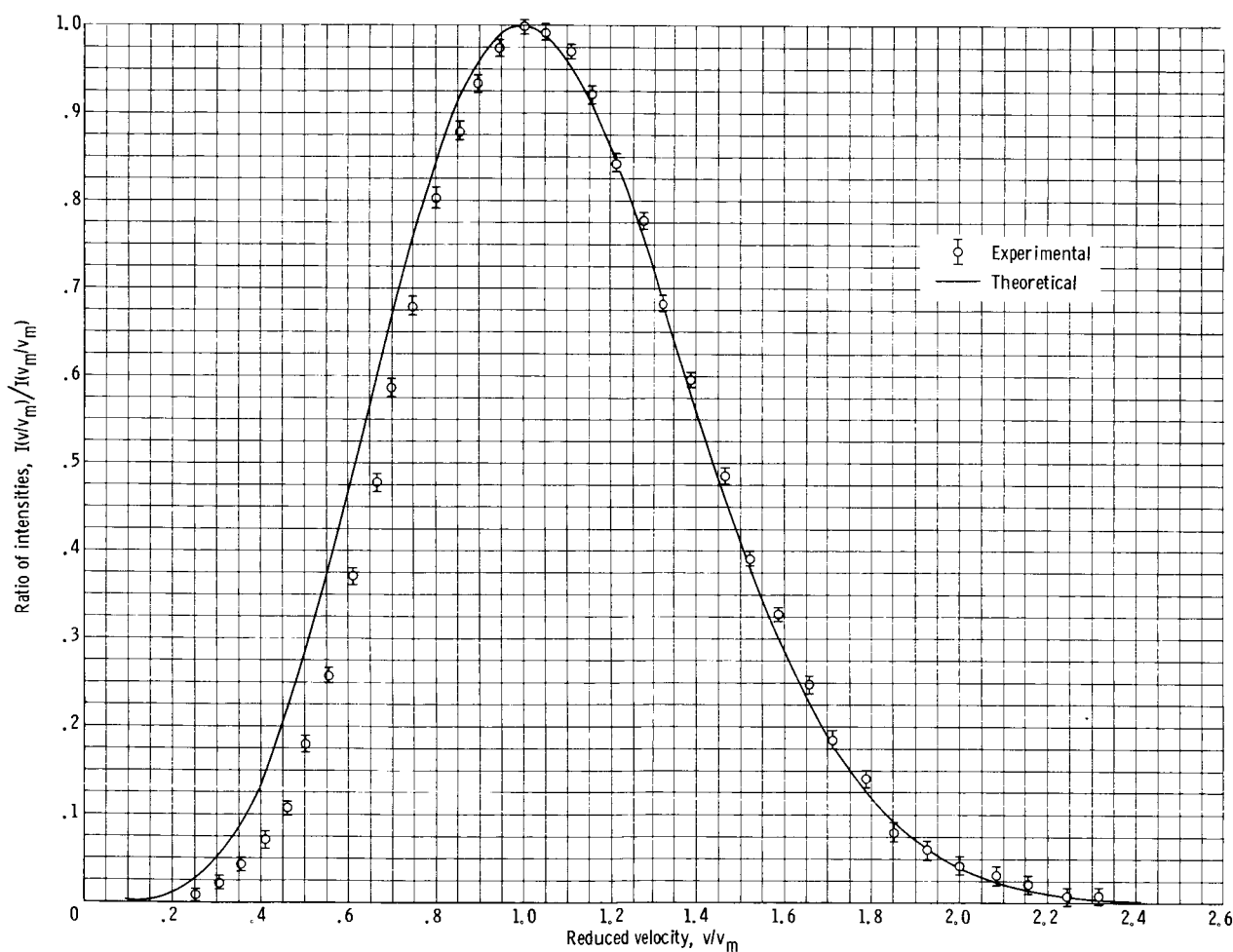$$v_m = \frac{2\pi L}{\varphi} \Omega_{max} \qquad (19)$$
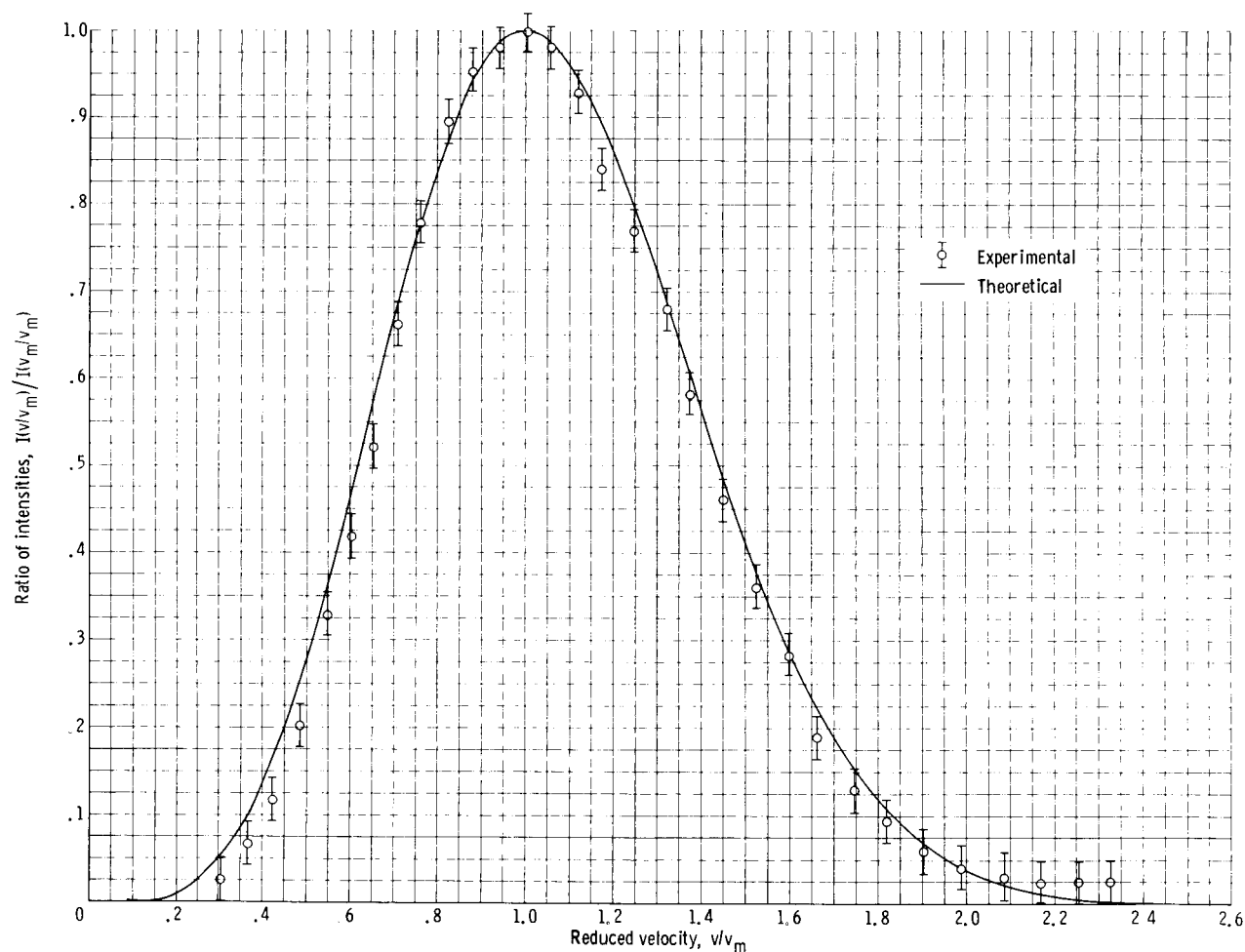
(a) Observed peak, 94.5 rps; source temperature, 444° K; oven slit width, 0.020 centimeter.

Figure 12. – Velocity distribution in atomic beam of cesium normalized to observed peak.

Combining equations (18) and (19) yields the following relation:

$$\varphi_{exp} = \pi L \left(\frac{m}{k}\right)^{1/2} \frac{\Omega_{max}}{T^{1/2}} \qquad (20)$$

Table II (p. 28) gives a comparison between the constants observed experimentally (φ_{exp} is obtained from equation (20) by using the experimentally observed Ω_{max} and the measured oven temperature T) and those calculated from the design equations of the selector. The observed φ_{exp} is consistently about 4.7 percent greater than the design value of 0.1695 radian. This is in agreement with the misalinement found in the third disk. In all subsequent discussions, the absolute velocity v is taken as that given by the experimentally determined value of $\varphi_{exp} = 0.1776$ radian. The velocity v, in centimeters per second, is given by

(b) Observed peak, 95 rps; source temperature, 464° K; oven slit width, 0.020 centimeter.

Figure 12. - Continued. Velocity distribution in atomic beam of cesium normalized to observed peak.

21

$$v = 3.54 \times 10^2 \Omega \hspace{4cm} (21)$$

where Ω is in rotations per second.

Using the experimentally determined value of φ, a new calculation of the geometric transmission of the velocity selector yields a value of $G = 0.0150$, in good agreement with the experimentally observed value of 0.0146.

OBSERVED VELOCITY DISTRIBUTIONS

Effects of Oven Slit Width, Source Pressure, and

Background Gas Scattering

The velocity-distribution data for a constant oven slit width shows that, as the oven temperature increases, corresponding to a greater beam source
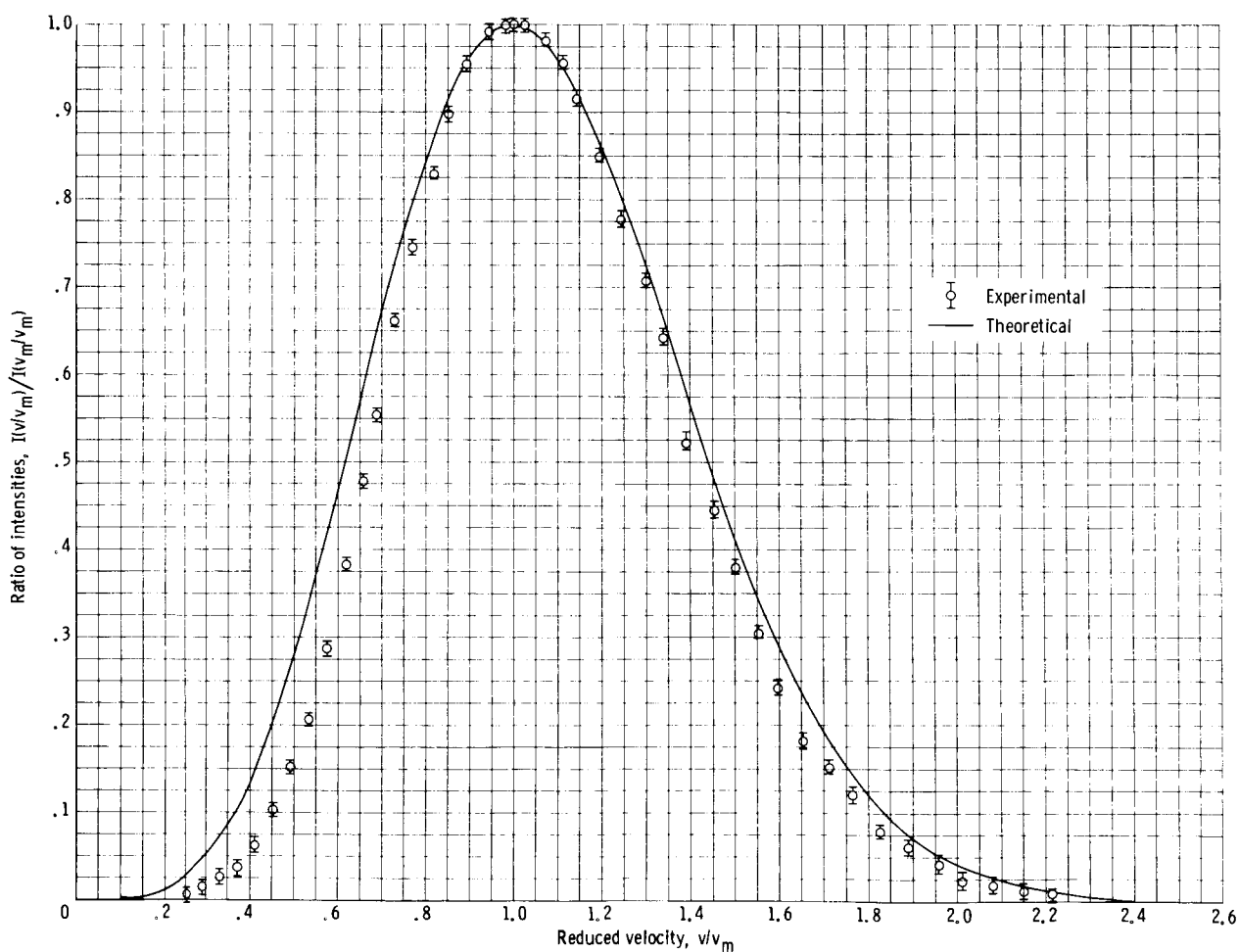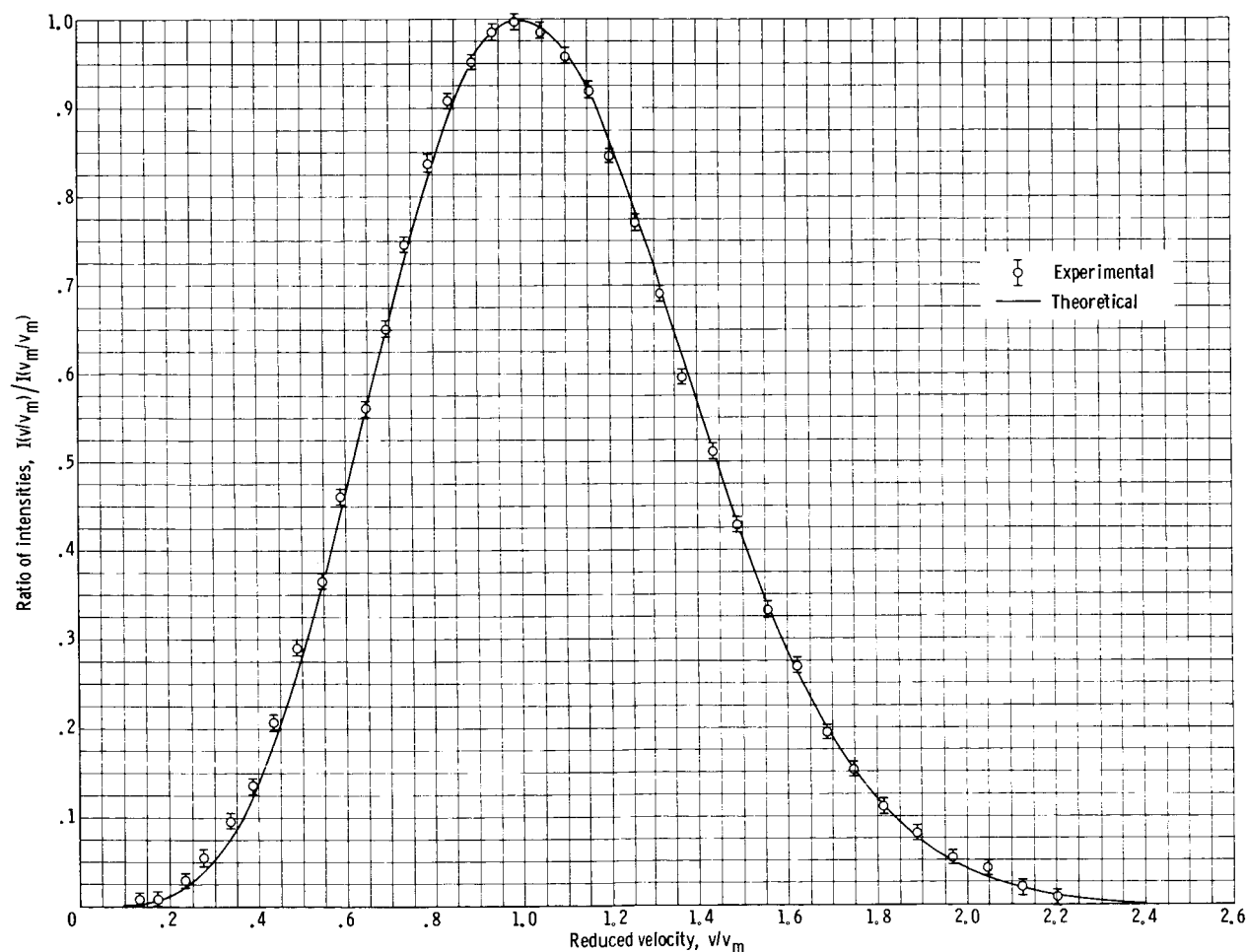

(c) Observed peak, 98.5 rps; source temperature, 473° K; oven slit width, 0.020 centimeter.

Figure 12. – Continued. Velocity distribution in atomic beam of cesium normalized to observed peak.

pressure, and hence a decreasing mean free path in the oven and near the slit assembly, the observed velocity distributions become more and more deficient in the slower velocities. This is in qualitative agreement with the formation of a cloud of beam atoms outside the oven slit. The cloud of beam atoms tends to alter the Maxwellian distribution because of the velocity dependence of the effective elastic scattering cross section. Figures 12(a) to (c), corresponding to an oven slit width of 0.020 centimeter and cesium pressures of 2.2×10^{-2} to 7.4×10^{-2} millimeter of mercury, illustrate this effect very graphically. At the highest source pressure investigated with an oven slit width of 0.020 centimeter, the observed distribution (fig. 12(c)) is highly non-Maxwellian on the low velocity side of the maximum and is also noticeably deficient in higher velocity atoms. The apparent high deficiency is due to the normalization of the experimental data to the observed peak velocity. A closer look (unpublished NASA data obtained by E. J. Manista of Lewis) at the effective scattering of the Maxwellian distribution by either residual gases along the beam path or by a cloud of beam atoms near the source slit, shows that atoms possessing the velocity of the vacuum peak are scattered out of the beam faster than those at

(d) Observed peak, 90 rps; source temperature, 411° K; oven slit width, 0.010 centimeter.

Figure 12. - Continued. Velocity distribution in atomic beam of cesium normalized to observed peak.

higher velocities. In other words, the passage of the beam through the scattering gas causes distortion in the original Maxwellian distribution and a shifting of the entire distribution toward higher velocities. Normalizing to the observed peak velocity in these cases tends to shift all the observed data points to the left, or toward reduced generalized velocities as is evidenced by figure 12(c). This shift amounts to less than a 2-percent correction to the data shown in figure 12(c) and becomes smaller as the source pressure and oven slit width are decreased. The deficiency of slower moving atoms, however, is clearly evident in figure 12(c). The deficiency varies from about 8 percent at a velocity corresponding to 0.75 of the maximum to over 45 percent at velocities less than 0.5 of the maximum. As the source pressure is lowered, thus decreasing the probability of cloud formation and beam scattering near the oven slit, this deficiency in the observed distributions becomes less. As can be seen from figure 12(a), there is no detectable deficiency in the distribution at a generalized velocity of 0.75. Furthermore, the deficiency at a velocity of 0.5 is now less than 18 percent.
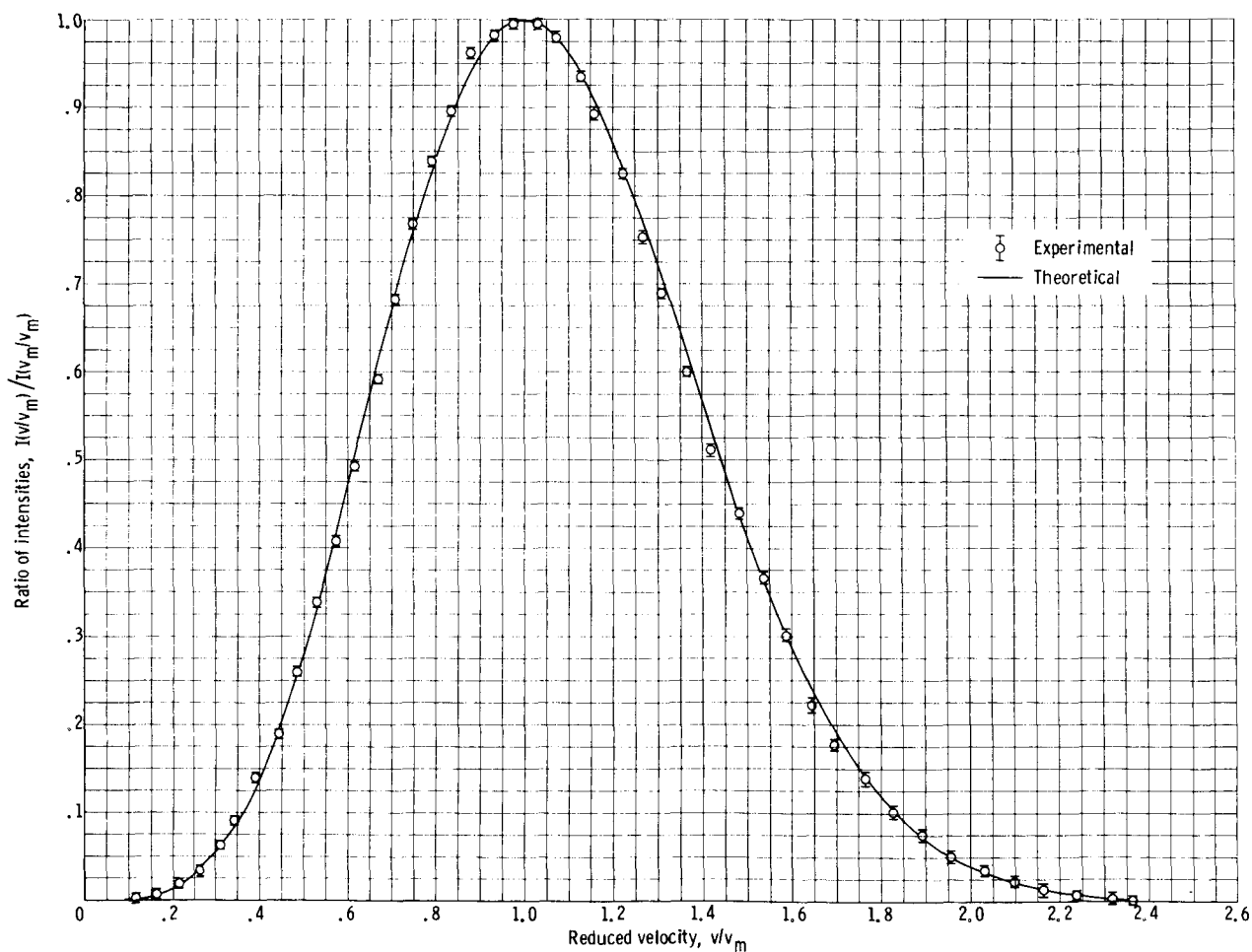
(e) Observed peak, 92.5 rps; source temperature, 431° K; oven slit width, 0.010 centimeter.

Figure 12. - Continued. Velocity distribution in atomic beam of cesium normalized to observed peak.

The data presented in figures 12(d) to (f) were taken with an oven slit width of 0.010 centimeter and at source pressures in the range of 4.6×10^{-3} to 3.2×10^{-2} millimeter of mercury. The observed distributions in figures 12(d) and (e) agree with the theoretical distributions over the entire velocity range within experimental errors. There is no apparent velocity shift of the distribution to higher velocities, as was noted in figure 12(c), nor is there any detectable deficiency of slower velocity atoms; however, as the source pressure was increased to 3.2×10^{-2} millimeter of mercury (fig. 12(f)) a detectable deficiency of the slower velocities became apparent. Moreover, the deficiency detected, 9 percent at $x = 0.5$, is less than that corresponding to an oven slit width of 0.020 centimeter and a typical source pressure of 2.2×10^{-2} millimeter of mercury (fig. 12(a)) where a deficiency of 18 percent was noted at the corresponding velocity.
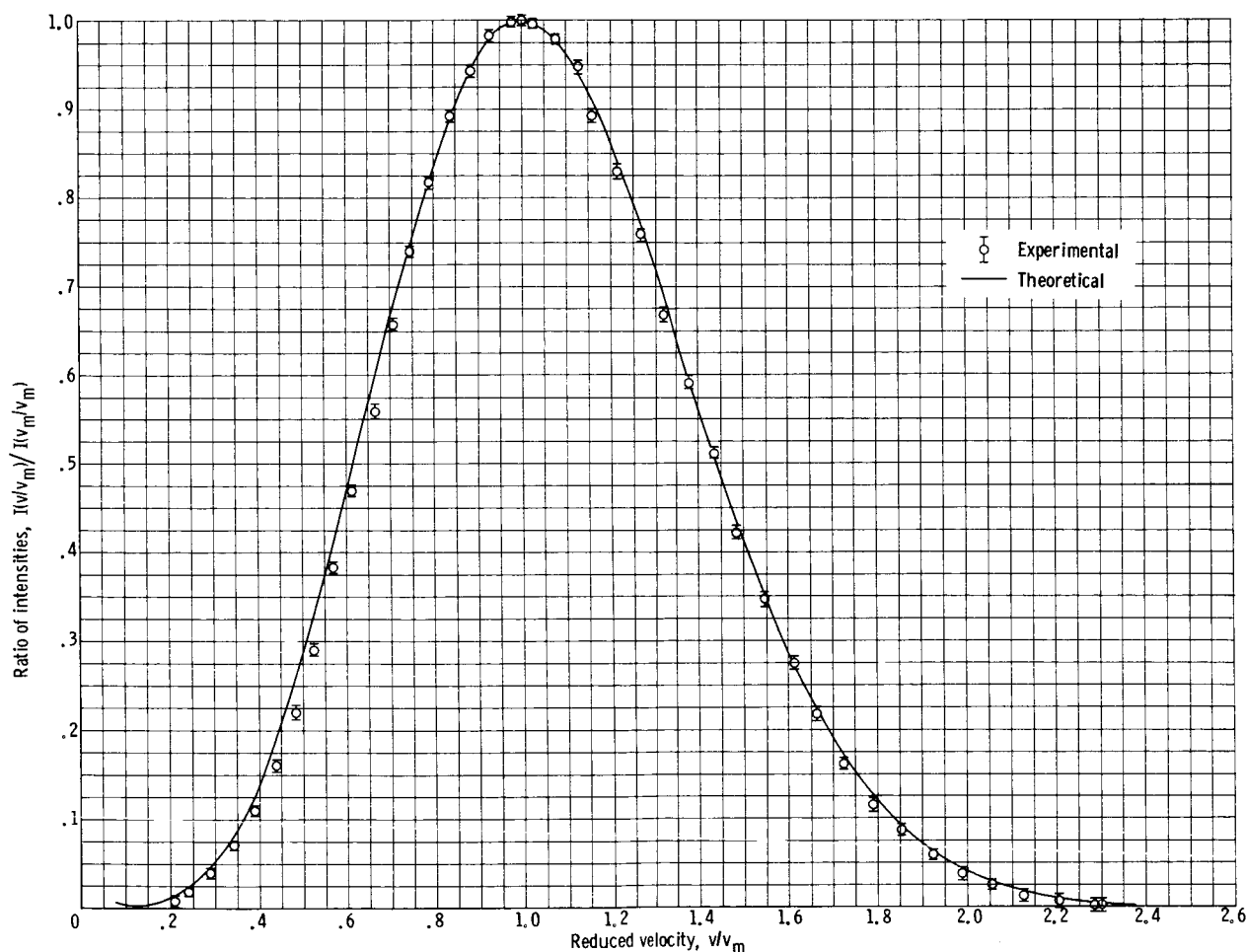
(f) Observed peak, 95 rps; source temperature, 452° K; oven slit width, 0.010 centimeter.

Figure 12. - Concluded. Velocity distribution in atomic beam of cesium normalized to observed peak.

Figure 13 shows the effect a scattering gas can have on the observed velocity distributions. The data presented correspond to the same experimental conditions of oven reservoir temperature and slit width as presented in figure 12(f), except that nitrogen gas was leaked into the chamber such that the total beam intensity was attenuated by about 50 percent of that of the "zero" nitrogen pressure case of figure 12(f). The observed experimental peak with 50 percent nitrogen attenuation was 100 rotations per second, while the experimental peak under zero percent attenuation was 95 rotations per second. The data in figure 13 are normalized to the zero scattering gas pressure maximum of 95 rotations per second to illustrate the real shift of the distribution to higher velocities (unpublished NASA data obtained by E. J. Manista of Lewis). The shift of the peak velocity in this case is about 5 percent.

EFFECTIVE SCATTERING CROSS SECTIONS OF CESIUM IN NITROGEN AND ARGON

The scattering data have been analyzed according to the method of Rosin and Rabi (ref. 13) to obtain an effective hard-sphere scattering cross section.
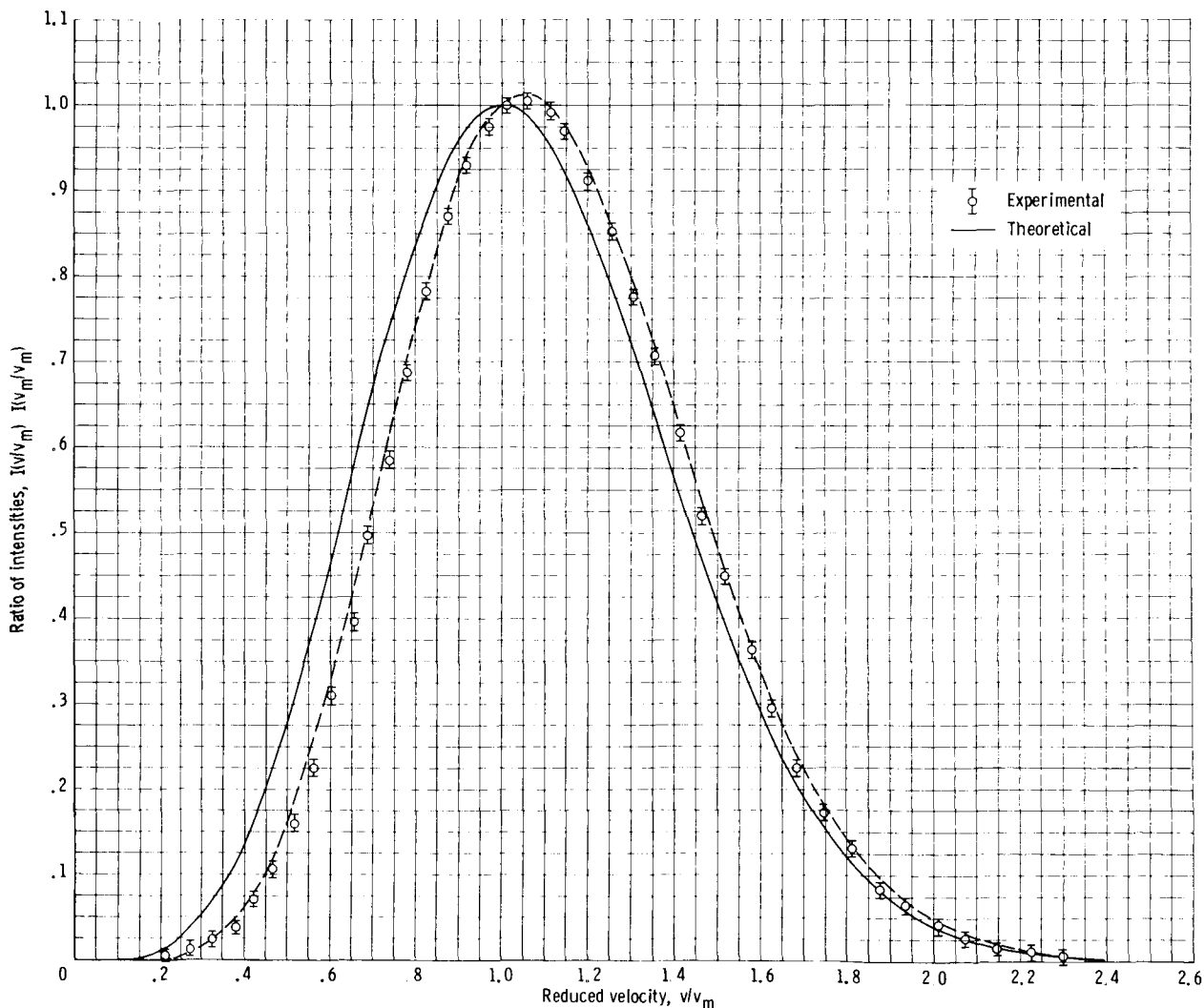

Figure 13. - Velocity distribution in attenuated atomic beam of cesium normalized to "vacuum" peak of 95 rps. Total beam intensity attenuated by about 50 percent; observed peak was actually 100 rps   Source temperature, 452° K; oven slit width, 0.010 centimeter; nitrogen scattering gas pressure, $\approx 6.3 \times 10^{-6}$ millimeter of mercury.

TABLE II. - COMPARISON OF OBSERVED VELOCITY-

SELECTOR CONSTANTS WITH DESIGN

Oven slit width, cm	Oven temper-ature, °K	Oven pressure, mm Hg	Slit offset angle, radians (a)	Transmis-sion (b)
0.020	473	7.4×10^{-2}	0.1784	------
	473	7.4×10^{-2}	.1803	0.0156
	464	5.2×10^{-2}	.1755	.0153
	444	2.2×10^{-2}	.1785	.0145
.010	391	1.6×10^{-3}	.1771	.0145
	390	1.5×10^{-3}	.1783	.0144
	412	4.9×10^{-3}	.1755	.0141
	411	4.6×10^{-3}	.1777	.0134
	411	4.6×10^{-3}	.1767	.0146
	432	1.3×10^{-2}	.1773	.0145
	452	3.2×10^{-2}	.1778	.0147
		Average:	0.1776	0.0146

[a]Calculated slit offset angle based on design
geometry, 0.1695 radian.

[b]Calculated transmission based on design
geometry, 0.0164; based on average observed
slit angle, 0.0150.

Five independent attenuations were obtained in each scattering gas to determine the hard-sphere cross section. Figure 14 is representative of the data taken with an oven slit width of 0.010 centimeter. The ordinate is the measured total beam current at a pressure p of the scattering gas normalized to the total beam current at zero pressure of the scattering gas. The abscissa is the true pressure of the scattering gas in millimeters of mercury measured by the calibrated ion gage. The data are presented for two independent attenuations each in nitrogen and argon to show the reproducibility of the experiment. The Cs-He attenuation is not shown because of the experimental difficulties involved in detecting helium at the low scattering gas pressures.

The probability P(v) that a beam atom of velocity v will travel a distance l from the oven slit to the detector without suffering a collision is given by
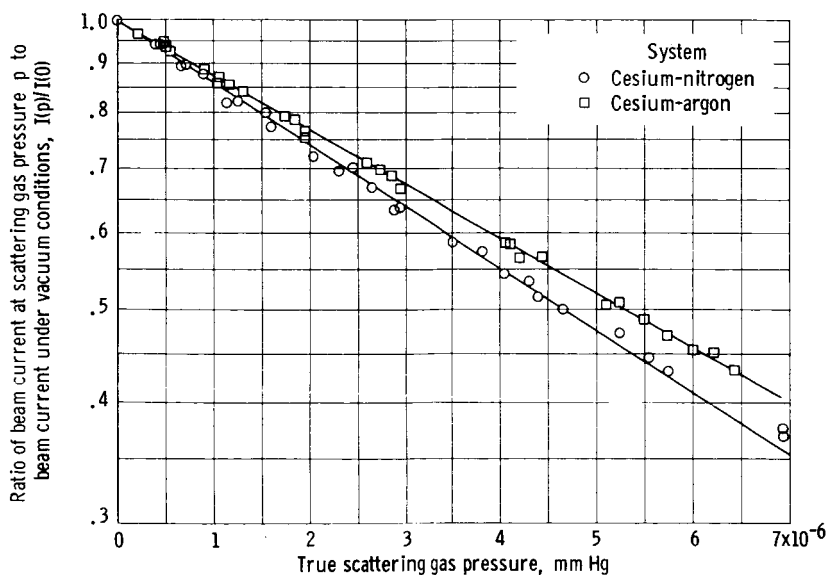
$$P(v) = e^{-l/\lambda(v)} \tag{22}$$

Figure 14. - Total cesium beam scattering. Cesium beam temperature, 447° K; scattering gas temperature, 293° K.

where $\lambda(v)$ is the mean free path for a velocity v. Since the mean free path is inversely proportional to the pressure,

$$p_0 \lambda_0(v) = p\lambda(v) \tag{23}$$

where p_0 and $\lambda_0(v)$ are constants in terms of the scattering gas density and p is the observed pressure. For a constant density of scattering particles throughout the beam length l,

$$P(v) = e^{-lp/p_0\lambda_0(v)} \tag{24}$$

Experimentally, one measures an effective $\langle p_0 \lambda_0 \rangle$ by determining the attenuation of the beam current as the pressure of the scattering gas is increased

$$\langle p_0 \lambda_0 \rangle = \frac{lp}{\ln \dfrac{I(0)}{I(p)}} \tag{25}$$

where $I(0)$ is the "vacuum" beam current and $I(p)$ is the measured beam current at a pressure p of the scattering gas.

Following Rosin and Rabi, a suitable collision frequency and hence a suitable value of $\lambda_0(v)$ is obtained by averaging the collision probability over the scattering-gas velocity distribution in terms of an effective hard-sphere cross section $\pi\sigma_{AG}^2$. The subscript A refers to the beam atom and the subscript G to the scattering gas. The number of collisions made per second by a beam atom of velocity v_A with molecules of the scattering gas is

$$\Theta = \pi^{1/2}\sigma_{AG}^2 n_G \frac{2kT_G}{m_G} \frac{\psi\left[v_A\left(\dfrac{m_G}{2kT_G}\right)^{1/2}\right]}{v_A} \tag{26}$$

where n_G is the number of scattering gas atoms per cubic centimeter at a temperature of T_G, σ_{AG} is the effective collision radius in centimeters, k is the Boltzmann constant, T_G is the absolute temperature, m_G is the molecular mass, and v_A is the molecular velocity. The function $\psi\left[v_A\left(\dfrac{m_G}{2kT_G}\right)^{1/2}\right]$ is given by

$$\psi(x) = xe^{-x^2} + (1 + 2x^2)\int_0^x e^{-y^2}\,dy \tag{27}$$

and has been tabulated by Rosenberg (ref. 14) along with other functions related to Tait's definition of a mean free path (ref. 15). The mean free path of the atom through the scattering gas is then v_A/Θ. In total beam measurements, the preceding collision frequency must also be averaged over the velocity distribution of the beam particles. This averaging process yields the following equation for the effective mean free path

$$\lambda_o = \frac{2}{\pi^{1/2} n_G \sigma_{AG}^2} \left(\frac{m_A T_G}{m_G T_A}\right)^2 \int_0^\infty \frac{x^5 e^{-(m_A T_G/m_G T_A)x^2}}{\psi(x)} dx \qquad (28)$$

and for the effective collision radius

$$\sigma_{AG}^2 = \frac{3.42 \times 10^{-17}}{\langle p_o \lambda_o \rangle} F(\xi) \qquad (29)$$

where $\langle p_o \lambda_o \rangle$ is determined from experiment $\xi = \frac{m_A}{m_G}\frac{T_G}{T_A}$, and $F(\xi)$ is defined by

$$F(\xi) = \xi^2 \int_0^\infty \frac{x^5 e^{-\xi x^2}}{\psi(x)} dx \qquad (30)$$

and has been computed by Rosenberg (ref. 14).

Values of $\langle p_o \lambda_o \rangle$ were computed according to equation (25) for at least six different pressures corresponding to attenuations ranging from 25 to 80 percent of the vacuum beam. The values of $\langle p_o \lambda_o \rangle$ remained constant over the attenuation range investigated, as is indicated by the linearity of the data presented in figure 14.

TABLE III. - CESIUM-NITROGEN EFFECTIVE HARD-SPHERE CROSS SECTION

[Nitrogen gas temperature, 293° K.]

Beam temperature, °K	$\langle p_o \lambda_o \rangle$, (mm Hg)(cm)	$F(\xi)$	σ_{AG}, cm	$\pi \sigma_{AG}^2$, sq cm	Angular resolution, min	Source
447	2.34×10^{-4}	0.154	15.0×10^{-8}	710×10^{-16}	3.2	-------
---	2.16	-----	17.2	936	.08	Ref. 16
450	----	-----	16.1	814	2.0	Ref. 17
---	----	-----	17.0	908	---	Ref. 18

Table III gives the results of the nitrogen attenuation experiments. Other values of the Cs-N_2 interaction reported in the literature are those of Estermann, et al. (ref. 16), Rothe and Bernstein (ref. 17), and Pauly (ref. 18) and have been included for comparison. The larger values obtained by Estermann, et al. (ref. 16) and Pauly (ref. 18) are a predictable result of their smaller angular resolution.

A cross section of 700×10^{-16} square centimeter was measured for the Cs-Ar interaction. This value is consistent with the measurement of Rothe and Bernstein (ref. 17) of 857×10^{-16} square centimeter when the difference in angular resolution between their apparatus and the present one is taken into account. The present determination, however, along with the measurement of Rothe and Bernstein is in significant disagreement with the previous result of Rosin and Rabi (ref. 13), who found a value of only 572×10^{-16} square centimeter for

the Cs-Ar interaction. The discrepancy of the present result with that of Rosin and Rabi is not clear. Our relative value of the Cs-N_2 to the Cs-Ar cross section is 1.0 and is in good agreement with the 0.95 value found by Rothe and Bernstein (ref. 17).

CONCLUDING REMARKS

An atomic-beam apparatus has been designed and constructed for the study of velocity dependent total collision cross sections at thermal energies. The beam may be velocity selected over the range of 7×10^3 to 1×10^5 centimeters per second to provide an intense, monoenergetic (velocity spread at half-maximum calculated ≈ 5 percent) beam of atoms.

The effect of atomic scattering by a cloud of beam atoms near the source slit was investigated by observing the velocity distributions presented in a beam of cesium atoms for slit widths of 0.010 and 0.020 centimeter and under varying source pressures in the range of 1.5×10^{-3} to 7.4×10^{-2} millimeter of mercury. Deficiencies in the lower velocity groups were found over almost the entire range of source pressures for the 0.020-centimeter-wide slit and was attributed to cloud formation. No appreciable deficiencies in the lower velocity groups were detected in the case of the 0.010-centimeter-wide slit for source pressures below 1×10^{-2} millimeter of mercury. It was shown that apparent deficiencies in the higher velocity groups can arise from the normalization procedure used to reduce the experimental data for comparison with a normalized Maxwellian distribution.

Absolute total collision cross sections for the Cs-N_2 and Cs-Ar interactions were measured by total beam attenuations with an angular resolution of 3.2 minutes. The cesium beam temperature was 447° K and the scattering gas temperature was 293° K. A "hard-sphere" cross section of 710×10^{-16} square centimeter was measured for the Cs-N_2 interaction and a cross section of 700×10^{-16} square centimeter for the Cs-Ar interaction. The absolute values of the cross sections are accurate to ±10 percent.

Lewis Research Center
   National Aeronautics and Space Administration
      Cleveland, Ohio, October 8, 1964

REFERENCES

1. Ramsey, Norman Foster: Molecular Beams. Clarendon Press (Oxford), 1956.

2. Estermann, I.: Molecular Beam Technique. Rev. Modern Phys., vol. 18, July 1946, pp. 300-322.

3. Miller, R. C., and Kusch, P.: Velocity Distributions in Potassium and Thallium Atomic Beams. Phys. Rev., vol. 99, no. 4, Aug. 1955, pp. 1314-1321.

4. Estermann, I., Simpson, O. C., and Stern, O.: The Free Fall of Atoms and the Measurement of Velocity Distribution in a Molecular Beam of Cesium Atoms. Phys. Rev., vol. 71, no. 4, Feb. 1947, pp. 238-248.

5. Hostettler, Hans U., and Bernstein, Richard B.: Improved Slotted Disk Type Velocity Selector for Molecular Beams. Rev. Sci. Instr., vol. 31, no. 8, Aug. 1960, pp. 872-877.

6. Peaslee, D. C., and Mueller, H.: Elements of Atomic Physics. Prentice Hall, Inc., 1955.

7. Datz, Sheldon, and Taylor, Ellison H.: Ionization on Platinum and Tungsten Surfaces. I. The Alkali Metals. Jour. Chem. Phys., vol. 25, no. 3, Sept. 1956, pp. 389-394.

8. Datz, S., Minturn, R. E., and Taylor, F. H.: Thermal Positive Ion Emission and the Anomalous Flicker Effect. Jour. Appl. Phys., vol. 31, no. 5, May 1960, pp. 880-883.

9. Roberts, Richard William: The Scattering of a Potassium Atomic Beam by a Crossed Beam of Bromine Molecules. Ph. D. Thesis, Brown Univ., 1959.

10. Blodgett, Katherine B., and Langmuir, Irving: The Design of Tungsten Springs to Hold Tungsten Filaments Taut. Rev. Sci. Instr., vol. 5, Sept. 1934, pp. 321-333.

11. Massey, H. S. W., and Burhop, E. H. S.: Free Paths and Transport Phenomena in Gases and the Quantum Theory of Collisions. Pt. I. Rigid Sphere Model. Proc. Roy. Soc. (London), ser. A, vol. 141, Aug. 1, 1933, pp. 434-453.

12. Massey, H. S. W., and Burhop, E. H. S.: Electronic and Ionic Impact Phenomena. Clarendon Press (Oxford), 1952.

13. Rosin, Seymour, and Rabi, I. I.: Effective Collision Cross Sections of the Alkali Atoms in Various Gases. Phys. Rev., vol. 48, no. 4, Aug. 1935, pp. 373-379.

14. Rosenberg, Paul: Evaluation of Functions Related to Tait's Mean Free Path. Phys. Rev., vol. 61, Apr. 1942, pp. 528-530.

15. Jeans, James: The Dynamical Theory of Gases. Dover Pub., 1954.

16. Estermann, I., Foner, S. N., and Stern, O.: The Mean Free Paths of Cesium Atoms in Helium, Nitrogen and Cesium Vapor. Phys. Rev., vol. 71, no. 4, Feb. 1947, pp. 250-257.

17. Rothe, Erhard W., and Bernstein, Richard B.: Total Collision Cross Sections for the Interaction of Atomic Beams of Alkali Metals with Gases. Jour. Chem. Phys., vol. 31, no. 6, Dec. 1959, pp. 1619-1627.

18. Pauly, H.: Further Cross Sections for Collisions Between Atoms, Zs. Angew. Phys., vol. 9, no. 12, Dec. 1957, pp. 600-606.